Velocity–space structures of distribution function in toroidal ion temperature gradient turbulence

INSTITUTE OF PHYSICS PUBLISHING and INTERNATIONAL ATOMIC ENERGY AGENCY NUCLEAR FUSION

Nucl. Fusion **46** (2006) 24–32 doi:10.1088/0029-5515/46/1/003

Velocity–space structures of distribution function in toroidal ion temperature gradient turbulence

T.-H. Watanabe and H. Sugama

National Institute for Fusion Science/The Graduate University for Advanced Studies, Toki, Gifu, 509-5292, Japan

Received 10 December 2004, accepted for publication 31 October 2005
Published 8 December 2005
Online at stacks.iop.org/NF/46/24

Abstract

Velocity–space structures of ion distribution function associated with the ion temperature gradient (ITG) turbulence and the collisionless damping of the zonal flow are investigated by means of a newly developed toroidal gyrokinetic-Vlasov simulation code with high velocity–space resolution. The present simulation on the zonal flow and the geodesic acoustic mode (GAM) successfully reproduces the neoclassical polarization of trapped ions as well as ballistic mode structures produced by collisionless particle motions. During the collisionless damping of GAM, the finer-scale structures of the ion distribution function in the velocity–space continue to develop while preserving an invariant defined by a sum of an entropy variable and the potential energy. The simulation results of the toroidal ITG turbulent transport clearly show generation of the fine velocity–space structures of the distribution function and their collisional dissipation. Detailed calculation of the entropy balance confirms the statistically steady state of turbulence, where the anomalous transport balances with the dissipation are given by the weak collisionality. The above results obtained by simulations with high velocity–space resolution are also understood in terms of generation, transfer and dissipation processes of the entropy variable in the phase–space.

PACS numbers: 52.25.Fi, 52.35.Ra, 52.65.Tt

1. Introduction

Numerical simulations based on the gyrokinetic formalism for drift wave turbulence, such as the ion temperature gradient (ITG) mode [1], have been extensively performed with the aim of understanding anomalous transport mechanism in a core region of magnetically confined plasmas. Transport suppression by self-generated zonal flows [2, 3] is one of the important results confirmed by the numerous simulations as well as the theoretical investigations. In a high-temperature plasma, where mean-free-paths of ions and electrons are much longer than device sizes, a perturbed part of the one-body velocity distribution function from the Maxwellian equilibrium, F_{M}, involves fine structures such as ballistic modes [4]. This is why kinetic approaches are indispensable for studying the core turbulent transport. Velocity–space structures of the distribution function and their relation to the turbulent transport, however, have rarely been discussed in the conventional kinetic simulations.

Regarding the velocity–space structures of f in plasma turbulence, it has been theoretically pointed out that, if a steady transport flux is observed in collisionless turbulence driven by constant density or temperature gradients, a quasisteady state should be realized [5–7], where high-order velocity–space moments of the perturbed distribution function δf continue to grow but the low-order ones are constant on average. Here, the deviation of f from the equilibrium is defined by $\delta f \equiv f - F_{\mathrm{M}}$. Our gyrokinetic-Vlasov (GKV) (or continuum gyrokinetic) simulation manifested the existence of the quasisteady state of the collisionless slab ITG turbulence [8], where the continuous generation of micro velocity–scale structures of δf through the ballistic mode is responsible for the growth of the high-order moments. The quasisteady state is also characterized by a balance between the monotonic increase of an entropy variable defined by a square-integral of δf and the turbulent transport. Recently, it has been shown numerically and analytically how the whole velocity–space spectrum of δf from macro to micro scales is determined by processes of the anomalous heat transport, the phase mixing, and the dissipation in the steady state of the weakly collisional slab ITG turbulence [9]. Since the macro velocity–space structures of f directly related to the turbulent transport flux are hardly influenced by collisions in the weak collisionality limit, the transport coefficient asymptotically approaches the value for the collisionless case for sufficiently low collision frequency. A logarithmic dependence of the transport on

relatively large values of ν has also been obtained [9]. It is emphasized that only a kinetic simulation with high velocity–space resolution and negligible numerical dissipation enables one to quantitatively investigate how the turbulent transport depends on the weak collisionality.

We have now developed a new toroidal GKV simulation code with high velocity–space resolution [10], which can precisely deal with the phase-mixing processes of f in toroidal configurations. With this code, detailed velocity–space structures produced by collisionless dynamics of the zonal flow [11] and the geodesic acoustic mode (GAM) [12] are successfully simulated and the transport flux in the toroidal ITG turbulence consistent with the entropy balance can be obtained. In this paper, we present the numerical simulation results of the zonal flow dynamics and the ITG turbulent transport in a tokamak configuration, focusing on the velocity–space structures of the ion distribution function.

This paper is organized as follows. After the introduction of the physical model in section 2, the balance equation for the entropy variable in a toroidal flux tube configuration is described in section 3. In section 4, we report velocity–space structures of δf during the collisionless damping of GAM associated with the zonal flow, the level of which is considered critical for the determination of the transport flux in the toroidal ITG turbulence. The nonlinear simulation results of the toroidal ITG turbulent transport are shown in section 5, where the entropy balance and the velocity–space structures of the distribution function are discussed. The results are summarized in section 6.

2. Model

We consider the gyrokinetic equation [13] for the ion distribution function in the low-β (electrostatic) limit. By applying the flute reduction for a large-aspect-ratio tokamak with concentric circular magnetic surfaces and the major radius R_0, the governing equation is written as

$$\frac{\partial \delta f}{\partial t} + v_\parallel \boldsymbol{b}\cdot\nabla\delta f + \frac{c}{B_0}\{\Phi, \delta f\} + \boldsymbol{v}_d\cdot\nabla\delta f - \mu(\boldsymbol{b}\cdot\nabla\Omega_i)\frac{\partial \delta f}{\partial v_\parallel} = (\boldsymbol{v}_* - \boldsymbol{v}_d - v_\parallel \boldsymbol{b})\cdot\frac{e\nabla\Phi}{T_\mathrm{i}}F_\mathrm{M} + C(\delta f) \tag{1}$$

where $\boldsymbol{b}$, B_0, c, Φ, e and T_i are the unit vector parallel to the magnetic field, magnetic field strength on the magnetic axis, the speed of light, the electrostatic potential averaged over the gyromotion, the elementary charge and the ion temperature, respectively. The perturbed gyrocentre distribution function for ions is denoted by δf. The parallel velocity, $v_\parallel$, and the magnetic moment, μ, are used as the velocity–space coordinates, where μ is defined by $\mu \equiv v_\perp^2/2\Omega_\mathrm{i}$ with the ion cyclotron frequency $\Omega_\mathrm{i} = eB/m_\mathrm{i}c$ (m_i is the ion mass) and the perpendicular velocity $v_\perp$. The collision term is shown by $C(\delta f)$. The Maxwellian distribution is given by

$$F_\mathrm{M} = n_0\left(\frac{m_\mathrm{i}}{2\pi T_\mathrm{i}}\right)^{3/2}\exp\left[-\frac{m_\mathrm{i}(v_\parallel^2 + 2\Omega_\mathrm{i}\mu)}{2T_\mathrm{i}}\right] \tag{2}$$

with poloidal angle dependence through Ω_i, since $v_\parallel$ and μ are chosen as the independent variables (the phase–space coordinates).

In the toroidal flux tube coordinates [14], $x = r - r_0$, $y = (r_0/q_0)[q(r)\theta - \zeta]$ and $z = \theta$ [where the safety factor $q(r = r_0) = q_0$ at the minor radius $r = r_0$], background gradients and magnetic shear parameters are assumed to be constant, such that $L_n = -(\mathrm{d}\ln n/\mathrm{d}r)^{-1}$, $L_T = -(\mathrm{d}\ln T_\mathrm{i}/\mathrm{d}r)^{-1}$ and $q(r) = q_0[1 + \hat{s}(r - r_0)/r_0]$. The poloidal and toroidal angles are denoted by θ and ζ, respectively. The abbreviations are defined by

$$\boldsymbol{b}\cdot\nabla = \frac{1}{q_0R_0}\frac{\partial}{\partial z}, \qquad \{\Phi, \delta f\} = \frac{\partial\Phi}{\partial x}\frac{\partial\delta f}{\partial y} - \frac{\partial\Phi}{\partial y}\frac{\partial\delta f}{\partial x},$$

$$B = B_0\left(1 - \frac{r_0}{R_0}\cos z\right),$$

$$\boldsymbol{v}_\mathrm{d}\cdot\nabla = -\frac{v_\parallel^2 + \Omega_{\mathrm{i}0}\mu}{\Omega_{\mathrm{i}0}R_0}\left[\sin z\frac{\partial}{\partial x} + (\cos z + \hat{s}z\sin z)\frac{\partial}{\partial y}\right],$$

$$\boldsymbol{v}_*\cdot\nabla = -\frac{cT_\mathrm{i}}{eL_nB_0}\left[1 + \eta_\mathrm{i}\left(\frac{m_\mathrm{i}v^2}{2T_\mathrm{i}} - \frac{3}{2}\right)\right]\frac{\partial}{\partial y},$$

where $\eta_\mathrm{i} = L_n/L_T$ and $v^2 = v_\parallel^2 + 2\Omega_\mathrm{i}\mu$. The radially-localized flux tube model enables us to impose the periodic boundary condition both in the x and y directions so that the Fourier spectral method can be applied to the calculation of the convection (the Poisson brackets) term in equation (1). In the perpendicular wave number space (k_x, k_y), Φ is related to the electrostatic potential, ϕ, such that

$$\Phi_{k_x,k_y} = J_0(k_\perp v_\perp/\Omega_\mathrm{i})\phi_{k_x,k_y}. \tag{3}$$

Here, J_0 is the zeroth order Bessel function and $k_\perp^2 = (k_x + \hat{s}zk_y)^2 + k_y^2$. The potential acting on particle positions, ϕ_{k_x,k_y}, is determined by the quasi-neutrality condition,

$$\int J_0 f_{k_x,k_y}\mathrm{d}^3v - \frac{e\phi_{k_x,k_y}}{T_\mathrm{i}}n_0(1 - \Gamma_0) = n_{\mathrm{e},k_x,k_y}, \tag{4}$$

where the Fourier component of δf is denoted by f_{k_x,k_y}. Also, $\Gamma_0 = \mathrm{e}^{-b}I_0(b)$ with $b = (k_\perp v_\mathrm{ti}/\Omega_\mathrm{i})^2$. The zeroth order modified Bessel function and the ion thermal speed are represented by I_0 and $v_\mathrm{ti} = \sqrt{T_\mathrm{i}/m_\mathrm{i}}$, respectively. The ratio of the electron density perturbation, n_{e,k_x,k_y}, to the averaged one, n_0, is assumed to be given in terms of the electron temperature, T_e, by

$$\frac{n_{\mathrm{e},k_x,k_y}}{n_0} = \begin{cases} \tau\dfrac{e(\phi_{k_x,k_y} - \langle\phi_{k_x,k_y}\rangle)}{T_\mathrm{i}} & \text{for } k_y = 0 \\ \tau\dfrac{e\phi_{k_x,k_y}}{T_\mathrm{i}} & \text{for } k_y \neq 0 \end{cases}, \tag{5}$$

where $\tau = T_\mathrm{i}/T_\mathrm{e}$ and $\langle\cdots\rangle$ means the flux surface average defined by

$$\langle A\rangle = \int_{-N_\theta\pi}^{+N_\theta\pi}\frac{A}{B_\mathrm{p}}\mathrm{d}z\Big/\int_{-N_\theta\pi}^{+N_\theta\pi}\frac{1}{B_\mathrm{p}}\mathrm{d}z = \int_{-N_\theta\pi}^{+N_\theta\pi}\frac{A}{B}\mathrm{d}z\Big/\int_{-N_\theta\pi}^{+N_\theta\pi}\frac{1}{B}\mathrm{d}z, \tag{6}$$

for $k_y = 0$. Here, the poloidal magnetic field is denoted by B_p. The last equality in equation (6) holds for the concentric circular magnetic surfaces with $\boldsymbol{B} = B(r,\theta)[\boldsymbol{e}_\zeta + (r/qR_0)\boldsymbol{e}_\theta]$,

by neglecting $O[(r/R_0)^2]$ terms, where $\boldsymbol{e}_\theta$ and $\boldsymbol{e}_\zeta$ denote the orthogonal unit vectors in the poloidal and toroidal directions, respectively. The parallel length of the flux tube is set to $2N_\theta\pi$ where the modified periodic boundary condition is used in the z direction [14]. Hereafter, physical quantities are normalized as follows: $x = x'/\rho_\mathrm{i}$, $t = t' v_\mathrm{ti}/L_n$, $v = v'/v_\mathrm{ti}$, $B = B'/B_0$, $\phi = e\phi' L_n/T_\mathrm{i}\rho_\mathrm{i}$ and $f = f' L_n v_\mathrm{ti}^3/\rho_\mathrm{i} n_0$, where prime means dimensional quantities and $\rho_\mathrm{i} = v_\mathrm{ti}/\Omega_{\mathrm{i}0}$ with $\Omega_{\mathrm{i}0} = eB_0/m_\mathrm{i}c$.

3. Entropy balance

Taking the velocity–space integral, summation over k_x and k_y, and the magnetic surface average of the Fourier-transformed form of equation (1) multiplied by $f_{-k_x,-k_y}/F_\mathrm{M}$, one can derive the entropy balance equation (normalized),

$$\frac{\mathrm{d}}{\mathrm{d}t}(\delta S + W) = \eta_\mathrm{i} Q_\mathrm{i} + D_\mathrm{i}, \tag{7}$$

by use of equations (4) and (5). Here, the entropy variable, δS, the potential energy, W, the ion heat transport flux, Q_i, and the collisional dissipation, D_i, are, respectively, defined as

$$\delta S = \sum_{k_x,k_y} \delta S_{k_x,k_y} = \frac{1}{2}\sum_{k_x,k_y}\left\langle \int \frac{|f_{k_x,k_y}|^2}{F_\mathrm{M}}\,\mathrm{d}^3v \right\rangle,$$

$$W = \sum_{k_x,k_y} W_{k_x,k_y} = \frac{1}{2}\sum_{k_x,k_y}[\langle(1-\Gamma_0+\tau)|\phi_{k_x,k_y}|^2\rangle - \tau|\langle\phi_{k_x,k_y}\rangle|^2\delta_{k_y,0}],$$

$$Q_\mathrm{i} = \sum_{k_x,k_y} Q_{\mathrm{i},k_x,k_y} = \frac{1}{2}\sum_{k_x,k_y}\left\langle \mathrm{i}k_y\phi_{-k_x,-k_y}\int v^2 J_0 f_{k_x,k_y}\,\mathrm{d}^3v\right\rangle,$$

$$D_\mathrm{i} = \sum_{k_x,k_y} D_{\mathrm{i},k_x,k_y} = \sum_{k_x,k_y}\left\langle\int\left[\left(J_0\phi_{-k_x,-k_y} + \frac{f_{-k_x,-k_y}}{F_\mathrm{M}}\right)C(f_{k_x,k_y})\right]\mathrm{d}^3v\right\rangle.$$

The entropy balance in the flux tube coordinates is represented in the same form as that in the slab ITG turbulence [9]. In the derivation of equation (7), the contribution of the second and fifth terms on the left-hand-side of equation (1) cancels out because of the z-dependence of F_M induced by the choice of the velocity–space coordinates, $(v_\parallel, \mu)$. A more general form of the entropy balance equation in a toroidal configuration is considered in [6] and [15].

Our slab ITG turbulence simulations with high velocity-space resolution have confirmed that the quasisteady state, $\mathrm{d}(\delta S)/\mathrm{d}t \approx \eta_\mathrm{i} Q_\mathrm{i}$, is realized in a collisionless turbulence with the statistically steady W and Q_i, where the monotonic increase of δS is attributed to the continuous generation of fine-scale structures of δf by the ballistic modes associated with the parallel advection term [8]. Contrarily, the statistically steady state of turbulence appears in a weakly collisional case, where $\eta_\mathrm{i} Q_\mathrm{i} \approx -D_\mathrm{i}$ and $\mathrm{d}(\delta S)/\mathrm{d}t \approx \mathrm{d}W/\mathrm{d}t \approx 0$, and is understood in terms of the production, transfer and dissipation processes of δS [9]. The steady and quasisteady states are, therefore, represented by two limiting cases of the entropy balance equation. It is purposed in the present paper to confirm the statistically steady state of the weakly collisional ITG turbulence in the toroidal flux tube configuration. The simulation results are shown in section 5.

It should be remarked that the weakly collisional turbulence can reach the statistically steady state in a much shorter time than the collision time $1/\nu$. Suppose that the collisionless particle motions incorporated with the stretching of δf due to the convective flow generate fine velocity–space structures of δf with a velocity scale of δv ($\ll v_\mathrm{ti}$). An effective dissipation rate of δf is estimated as $\nu_\mathrm{eff} \sim \nu(v_\mathrm{ti}/\delta v)^2 \sim \nu n$, where n ($\gg 1$) denotes order of the velocity moment that corresponds to the fine structure in the velocity space [9]. Thus, the statistically steady turbulence is realized in a time scale of $1/\nu_\mathrm{eff}$ ($\ll 1/\nu$).

According to the theory of entropy production, transfer, and dissipation processes for the slab ITG turbulence given in [9], the propagation time t_p of the entropy variable from the macro to the dissipation scale is given as follows. By considering a balance equation of the entropy variable at the nth order velocity moment, δS_n, one finds that

$$t_\mathrm{p} = \int_1^{n_\mathrm{d}} (J_n/\delta S_n)^{-1}\,\mathrm{d}n = \int_1^{\gamma/\nu}\frac{1}{2\gamma n}\,\mathrm{d}n = \frac{1}{2\gamma}\ln(\gamma/\nu).$$

Here, J_n represents the entropy transfer function in the n-space, and $n_\mathrm{d} = \gamma/\nu$ means the order of the velocity moment where the spectrum of the entropy variable exponentially decays due to the collisional dissipation (see [9] for more details). The exponential growth of the wave number of δf can be caused by the strain of the steady flow. The growth rate γ is estimated from the slab ITG turbulence simulation as $\gamma \sim 0.5$. It is also expected that the fluctuations of the n_dth order moments are dissipated with a time scale of $t_\mathrm{d} = 1/(2\nu n_\mathrm{d}) = 1/2\gamma$. Both the time scales, t_p and t_d, are much smaller than $1/\nu$ as expected in the above. Thus, the theoretical analysis agrees with the simulation results where the weakly collisional turbulence reaches the statistically steady state in a much shorter time than $1/\nu$.

The phase-mixing processes in a torus are more complicated than that in the slab geometry because of the toroidal magnetic drift and mirror motions as represented in equation (1). A power-law decay of a density perturbation due to the phase mixing caused by the toroidal drift [16], which can be precisely simulated by our toroidal flux tube code [10], is one of the examples. In the next section, we investigate the collisionless damping process of the zonal flow and the GAM by means of the GKV code, where the phase-mixing processes in the tokamak configuration as well as the mirror motion are taken into account. The time evolution of a zonal flow component with $k_y = 0$ (the toroidal mode number $n = 0$) is considered as an initial value problem of a linearized version of equation (1). The solution of the initial value problem is equivalent to the response kernel of the zonal flow to a source term [11]. The entropy balance equation for an axisymmetric component with a radial wave number k_x is written as

$$\frac{\mathrm{d}}{\mathrm{d}t}(\delta S_{k_x,0} + W_{k_x,0}) = D_{\mathrm{i},k_x,0}, \tag{8}$$

which corresponds to a subset of equation (7) with $k_y = 0$. During the collisionless ($D_{\mathrm{i},k_x,0} = 0$) damping of the zonal flow and GAM, thus, $G \equiv \delta S_{k_x,0} + W_{k_x,0}$ is invariant. It means that the decrease of the potential energy, $W_{k_x,0}$, due to the collisionless damping leads to the increase of the entropy variable, $\delta S_{k_x,0}$. It is, thus, expected that, according

to the enhancement of $\delta S_{k_x,0}$, fine-scale fluctuations of δf should develop in the phase space, while a coherent structure corresponding to the neoclassical polarization [11] can remain in association with the residual zonal flow level.

For precise reproduction of the entropy balance, high velocity–space resolution is necessary, since δS reflects fine-scale structures of δf which are artificially dissipated in numerical simulations with low resolution. (If the subgrid-scale fluctuations are not smoothed out, they will often cause the numerical instability.) The balance equation, equations (7) or (8), thus, offers a good way of judging whether the micro velocity–space structures consistent with the turbulent transport are correctly resolved or not.

4. Collisionless damping of zonal flow and GAM

The residual level of the zonal flow after the collisionless damping is considered to affect a saturation amplitude of the ITG turbulence [11]. Then, the initial value problem of the zonal flow and GAM, where a response function of a $k_y = 0$ mode is dealt with [11], has been investigated as an important benchmark test of toroidal gyrokinetic simulation codes [17, 18, 19, 20]. The conservation property given in equation (8) and the velocity–space profiles of the distribution function are useful for manifesting the physical mechanism of the collisionless damping of the zonal flow and the GAM as well as confirming the accuracy of the numerical simulations, while they have not been examined in the previous studies.

The collisionless damping of the GAM oscillation will be seen in the time-evolution of the zonal flow amplitude, $\langle\phi_{k_x,0}\rangle$, when the initial distribution function is given by the Maxwellian in equation (2) with $m = n = 0$, where m and n mean the poloidal and toroidal mode numbers, respectively. The time-history of $\langle\phi_{k_x,0}\rangle$ obtained by the toroidal flux tube simulation for the Cyclone DIII-D base case parameters [17] is shown in figure 1(*a*), where the radial wave number $k_x = 0.1715\rho_{\rm i}^{-1}$. The used parameters are as follows: $R_0/L_T = 6.92$, $\epsilon \equiv r_0/R_0 = 0.18$, $r_0/\rho_{\rm i} = 80$, $\hat{s} = 0.78$, $q_0 = 1.4$, $\eta_{\rm i} = 3.114$ and $\tau = 1$. For discretization of the velocity space, $-5v_{\rm ti} \leqslant v_\parallel \leqslant 5v_{\rm ti}$ and $0 \leqslant \mu \leqslant 12.5v_{\rm ti}^2/\Omega_{\rm i0}$, we have employed 1025×65 grid points, while 128 grid points are used for $-\pi \leqslant z < \pi$. Phase–space derivatives in the z and $v_\parallel$ directions are approximated by the fifth- and fourth-order finite difference, respectively. The numerical time-integration is calculated by the fourth-order Runge–Kutta–Gill method [21].

The residual level of $\langle\phi_{k_x,0}\rangle$ shown in figure 1(*a*) agrees well with the theoretical estimate, $\lim_{t\to\infty}\langle\phi_{k_x,0}(t)\rangle/\langle\phi_{k_x,0}(t=0)\rangle = 1/(1+1.6q^2/\epsilon^{1/2})$ [11]. The collisionless damping of the zonal flow and the GAM is caused by the phase mixing processes related to fine-scale structures of δf in the velocity space. According to equation (8), in the collisionless case, the entropy variable associated with the fine structures should increase so as to compensate the decrease of the potential energy. The simulation result shown in figure 1(*b*) confirms the entropy balance. During the collisionless damping of zonal flow and GAM with decrease of the potential energy, $W_{k_x,0}$, the entropy variable $\delta S_{k_x,0}$ increases while accurately preserving G. The high phase–space resolution enables us to reproduce the conservation of G with a relative error less than 3%.

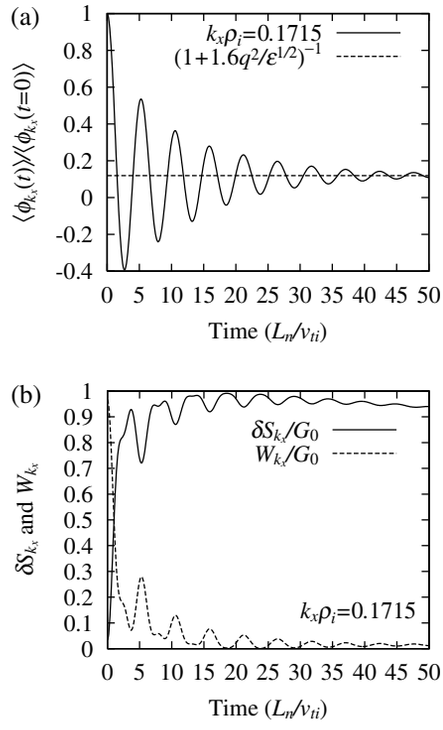

Figure 1. Time-evolutions of (*a*) the zonal flow potential, (*b*) the entropy variable, $\delta S_{k_x,0}$, and the potential energy, $W_{k_x,0}$, obtained by the toroidal flux tube simulation of the collisionless damping of the axisymmetric ($n = 0$) mode, where $G_0 = \delta S_{k_x,0} + W_{k_x,0}$ at $t = 0$.

The analytical solution for the zonal-flow component of the perturbed gyrocentre distribution function is given by

$$f_{k_x,0}(t) = F_{\rm M}\frac{e\langle\phi_{k_x,0}(0)\rangle}{T_{\rm i}}[k_x^2\rho_{\rm i}^2 + \{{\rm i}k_x(\overline{\rho_b} - \rho_b) + k_x^2(\rho_b\overline{\rho_b} - \tfrac{1}{2}\overline{\rho_b^2} - \tfrac{1}{2}\rho_b^2)/(1 + 1.6q^2/\epsilon^{1/2})], \tag{9}$$

where $\rho = v_\perp/\Omega_{\rm i}$, $\rho_b = (q/\epsilon)(v_\parallel/\Omega_{\rm i})$,

$$\overline{\rho_b} = \begin{cases} 0 & \text{for trapped particles,} \\ \pi(q/\epsilon\Omega_{\rm i0})(\mu\Omega_{\rm i0}\epsilon)^{1/2}\kappa/K(\kappa^{-1}) & \\ & \text{for passing particles,} \end{cases} \tag{10}$$

$$\overline{\rho_b^2} = \begin{cases} 4(q/\epsilon\Omega_{\rm i0})^2(\mu\Omega_{\rm i0}\epsilon)[E(\kappa)/K(\kappa) - 1 + \kappa^2] & \\ \qquad \text{for trapped particles} & \\ 4(q/\epsilon\Omega_{\rm i0})^2(\mu\Omega_{\rm i0}\epsilon)\kappa^2 E(\kappa^{-1})/K(\kappa^{-1}) & \\ \qquad \text{for passing particles} & \end{cases} \tag{11}$$

and $\kappa^2 = [v^2/2 - \mu\Omega_{\rm i0}(1-\epsilon)]/(2\mu\Omega_{\rm i0}\epsilon)$. Here, K and E denote the complete elliptic integrals of the first and second kinds, respectively. The bounce average is denoted by $\overline{\cdots}$, where the integral goes over a closed orbit for trapped particles but once around the poloidal circumference for passing particles. The above analytical solution is derived by using the expression for the gyrocentre distribution function $f_{\boldsymbol{k}}(t) = -J_0(e\phi_{\boldsymbol{k}}(t)/T_{\rm i})F_{\rm M} + g_{\boldsymbol{k}}(t)$ with $\phi_{\boldsymbol{k}}(t)$ and $g_{\boldsymbol{k}}(t)$ given by the Rosenbluth–Hinton theory [11], which describes the long-time behaviour of the zonal flow and drops out rapid oscillations such as the GAM.

Velocity–space profiles of Re$[f_{k_x,0}]$ at different time steps normalized by the initial zonal flow amplitude, $\langle\phi_{k_x,0}(t=0)\rangle$, are shown in figure 2, where the boundary of trapped and

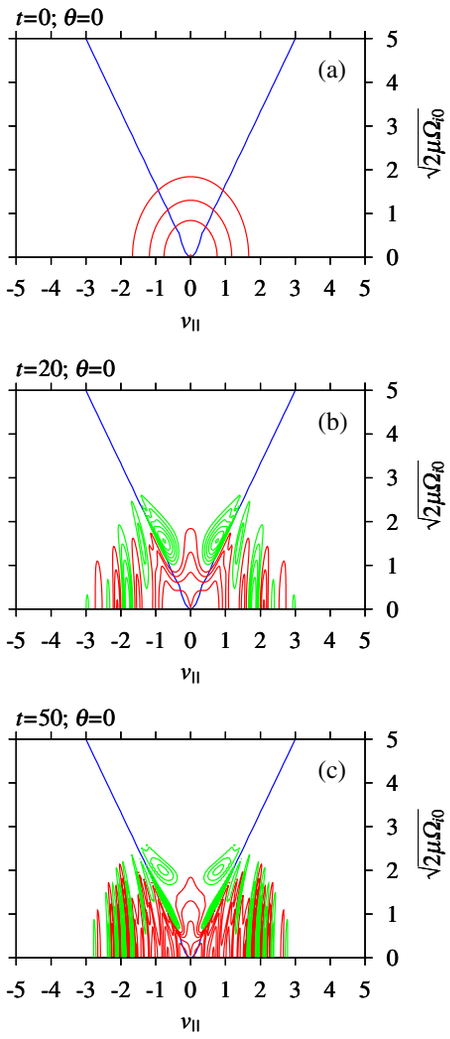

Figure 2. Velocity–space profiles of real part of the perturbed distribution function at $\theta = 0$ for different time steps of simulation. The amplitude is normalized by the initial zonal flow potential, $\langle\phi_{k_x,0}(t=0)\rangle$. The horizontal and vertical axes are defined by $v_\parallel$ and $\sqrt{2\mu\Omega_{i0}}$, respectively, where μ is the magnetic moment. Positive and negative parts are coloured by red and green, respectively, with the contour interval of 5×10^{-4}. Blue lines show the boundary of trapped and passing particles.

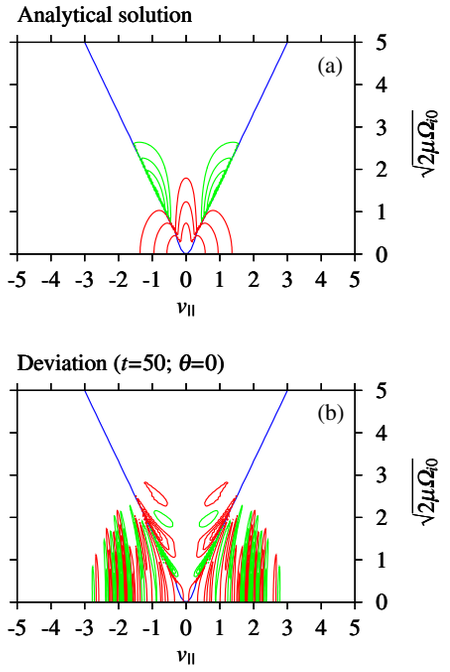

Figure 3. A velocity–space profile of real part of the perturbed distribution function at $\theta = 0$ given by (*a*) the analytical solution in equation (9) and (*b*) the difference of figure 2(*c*) from figure 3(*a*). Format of the plots is the same as those in figure 2.

passing ions is represented by blue lines. The contribution of the trapped ions to the neoclassical polarization [11] is clearly identified by a mean negative value of $f_{k_x,0}$ for trapped particles. The mean part of the distribution function resulting from the numerical simulation agrees with the analytical solution given by equation (9) [see also figure 3(*a*)], while the fine-scale fluctuations are caused by collisionless particle motions. For comparison with figure 2(*c*), the deviation of $f_{k_x,0}$ at $t = 50$ from the analytical solution is plotted in figure 3(*b*), where the fine structures of the trapped ion distribution are also found near the boundary between the trapped and passing regions. Generating fine-scale structures of $f_{k_x,0}$ in the direction of the parallel velocity ($v_\parallel$), the ballistic motion of the passing particles largely deforms the initial Maxwellian distribution as seen in figure 2, and results in the damping of GAM. The increase of $\delta S_{k_x,0}$ balancing with the decrease of $W_{k_x,0}$ stems from the development of the fine-scale fluctuations of $f_{k_x,0}$ in the velocity space. The continuous development of fine-scale structures of $f_{k_x,0}$ represents the transfer of the entropy variable from macro to micro velocity-scales, while the growth of $\delta S_{k_x,0}$ is saturated at a constant level after $t = 20L_n/v_{ti}$ [see figure 1(*b*)].

5. Toroidal ITG Turbulence

Nonlinear GKV simulations of the toroidal ITG turbulence are carried out by means of the flux tube model described in section 2. Parameters used are the same as those in section 4 but with finite collisionality. We have employed a collision operator given by the gyrophase (φ) average of the Lenard–Bernstein model, C_{LB}, [22] such as

$$C(f_{k_x,k_y}) = \frac{1}{2\pi}\int_0^{2\pi} \mathrm{d}\varphi\, \mathrm{e}^{\mathrm{i}L} C_{LB}(f_{k_x,k_y}\mathrm{e}^{-\mathrm{i}L})$$
$$= \nu_{ii}\left[\frac{1}{v_\perp}\frac{\partial}{\partial v_\perp}\left(v_\perp\frac{\partial f_{k_x,k_y}}{\partial v_\perp} + \frac{v_\perp^2}{v_{ti}^2}f_{k_x,k_y}\right)\right.$$
$$\left. + \frac{\partial}{\partial v_\parallel}\left(\frac{\partial f_{k_x,k_y}}{\partial v_\parallel} + \frac{v_\parallel}{v_{ti}^2}f_{k_x,k_y}\right) - \frac{k_\perp^2}{\Omega_i^2}f_{k_x,k_y}\right], \quad (12)$$

where ν_{ii} denotes the ion–ion collision frequency and $L = (k_\perp v_\perp/\Omega_i)\cos\varphi$ [23]. In the derivation of equation (12), we have omitted a part of the variation of the particle distribution which stems from the polarization due to the potential perturbation [23]. The contribution of the neglected part to the collision term is smaller than that considered in equation (12) because of the difference in the velocity scale.

Colour contour plots of the electrostatic potential perturbations obtained by the toroidal ITG turbulence simulation are shown in figure 4 for three different time moments, where $\nu_{ii} = 10^{-3}v_{ti}/L_n$ (banana regime where $\nu^* \equiv \nu_{ii}/(v_{ti}/q_0R_0)\epsilon^{3/2} \approx 0.04$), $N_\theta = 4$, $k_{x,\min} = 0.1715$,

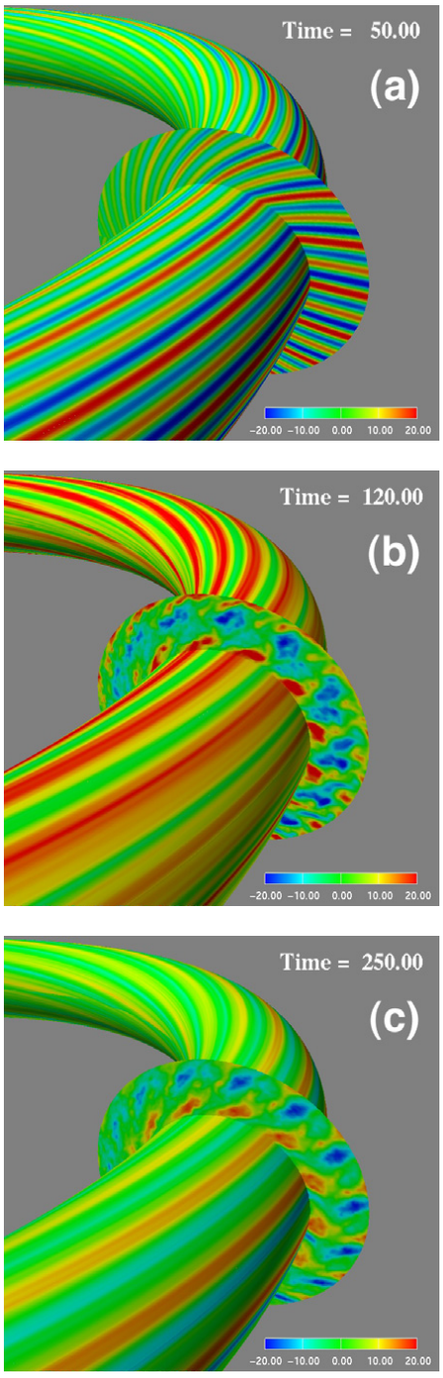

Figure 4. Colour contours of the electrostatic potential obtained by the toroidal ITG turbulence simulation at (*a*) $t = 50$, (*b*) 120 and (*c*) $250L_n/v_{\rm ti}$, where only a part of the flux tube in the range of $-\pi \leqslant z \leqslant \pi$ is plotted.

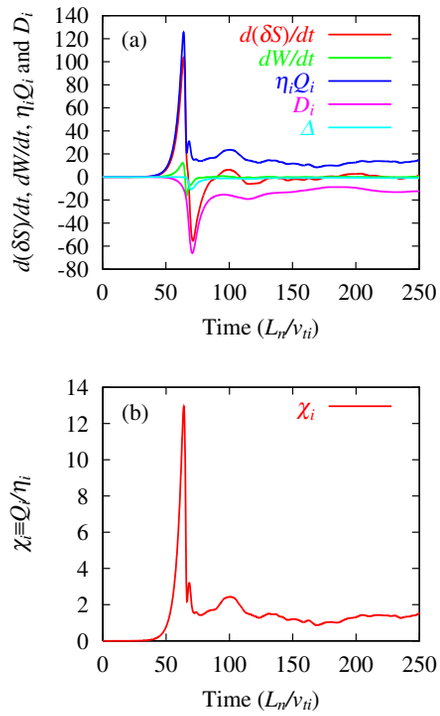

Figure 5. Time-evolutions of (*a*) the entropy balance and (*b*) the ion thermal transport coefficients $\chi_{\rm i}$ obtained by the toroidal ITG turbulence simulation.

$k_{x,\max} = 5.145$, $k_{y,\min} = 0.175$ and $k_{y,\max} = 1.75$ (31×21 Fourier components are involved in the k_x–k_y space, excluding their complex conjugates as well as modes employed for de-aliasing). The minimum values of k_x and k_y correspond to $\Delta q = 0.5$ and $N_\alpha = 10$, respectively, where Δq denotes a difference of the safety factor across the radial width. The toroidal periodicity of N_α is also assumed [14]. In a latter phase of the linear growth of the ITG instability ($t \approx 60L_n/v_{\rm ti}$), the zonal flow components are spontaneously excited, and reduce the turbulence level. As seen in figure 4, vortices with larger scales than that of the linearly most unstable mode dominate in the turbulence and are mainly responsible for the ion heat transport. A statistically steady turbulence with finite amplitudes of zonal flows is observed after $t \approx 120L_n/v_{\rm ti}$.

The entropy balance in the ITG turbulence simulation is shown in figure 5(*a*), where time-histories of four terms in equation (7) are plotted. The relative error $\Delta/D_{\rm i}$ [defined by $\Delta \equiv {\rm d}(\delta S{+}W)/{\rm d}t - \eta_{\rm i}Q_{\rm i} - D_{\rm i}$] in the saturated turbulence after $t \approx 80L_n/v_{\rm ti}$ is suppressed at 7–8% by use of high resolution, where 960 and 129×48 grid points are employed in the z- and $v_\parallel$–$v_\perp$ space, respectively. Better balancing of equation (7) is found for finer grid spacings, Δz, $\Delta v_\parallel$ and $\Delta v_\perp$, or for higher collision frequency, $\nu_{\rm ii}$, since fine-scale fluctuations of δf generated in the turbulence are damped by collisions. In the steady turbulence, the collisional dissipation nearly balances with the transport flux, $\eta_{\rm i}Q_{\rm i} \approx -D_{\rm i}$, in the same way as seen in the slab ITG simulation [9]. The ion heat transport coefficient, $\chi_{\rm i} \equiv Q_{\rm i}/\eta_{\rm i}$, is shown in figure 5(*b*), where the time-averaged value of $\chi_{\rm i} \approx 1.4\rho_{\rm i}^2 v_{\rm ti}/L_n$ from $t = 200$–$250L_n/v_{\rm ti}$ in the saturated turbulence is comparable with the results of other gyrokinetic simulations for the Cyclone base case ($\chi_{\rm i} \sim 2\rho_{\rm i}^2 v_{\rm ti}/L_n$) [17].

A quantitative estimate of the transport flux by means of collisionless or weakly collisional turbulence simulations, generally speaking, may suffer from a numerical error unless enough resolution for the velocity space is employed, as has been demonstrated in [10] where the transport flux is artificially increased in cases with insufficient velocity–space resolution. The entropy balance is a useful benchmark test for checking the soundness of simulation results as considered above. Introduction of the numerical diffusion may contribute to the reduction of the aliasing error, while the convergence of the transport coefficient against the artificial dissipation

should be thoroughly evaluated in the same way as the systematic study of the collisionality dependence given in [9] where χ_i asymptotically approaches the collisionless result for sufficiently low collision frequency but has a logarithmic dependence on relatively large values of ν_{ii}. In cases with insufficient resolution, therefore, one may overestimate the transport coefficient unless the numerical simulation result is independent of the magnitude of the artificial dissipation. Nevertheless, it is not obvious whether χ_i obtained by conventional gyrokinetic simulations with less velocity–space resolution than ours (e.g. see [19]) suffers from the numerical dissipation or not, since it depends on detailed techniques for treating the fine-scale fluctuations in each simulation code. Thus, a benchmark test for the entropy balance as given above or a systematic convergence study is desired in order to establish a reliable reference for numerical simulations of the kinetic plasma turbulent transport.

The balance relation, $\eta_i Q_i \approx -D_i$, suggests that fine-scale structures of δf generated by the ballistic mode in the turbulence are dissipated by the finite collisionality. Velocity–space profiles of $\mathrm{Re}(f_{k_x,k_y}/\phi_{k_x,k_y})$ observed at $t = 250L_n/v_{ti}$ are shown in figure 6 for the longest wavelength mode ($k_y = 0.175\rho_i^{-1}$), the linearly most unstable mode ($k_y = 0.35\rho_i^{-1}$) and a stable mode ($k_y = 0.7\rho_i^{-1}$), where $\theta = z = 0$ and $k_x = 0$. The distribution function of the linear stable mode with $k_y = 0.7\rho_i^{-1}$ mainly consists of small scale structures in the velocity space. As seen in cross-sectional plots of f_{k_x,k_y} at $t = 50$ (linear growth phase) and $250L_n/v_{ti}$ (nonlinear saturation phase) in figure 7, the velocity–space profile of $\mathrm{Re}(f_{k_x,k_y})$ for the dominant long wavelength mode ($k_y = 0.175\rho_i^{-1}$) is similar to that of the linear unstable eigenfunction. The same feature of f_{k_x,k_y} has also been observed in the slab ITG turbulence simulations [8]. This means that the entropy variable produced in the macro velocity–scale by the unstable modes is transferred to and is dissipated in the micro scales by the finite collision.

It is remarked that the present GKV simulation with high velocity–space resolution enables one to quantitatively study the entropy balance in the five-dimensional phase–space in association with the toroidal ITG turbulent transport. The simulation result of the toroidal ITG turbulence confirms the scenario on the steady state of the entropy balance originally derived from the slab ITG turbulence simulations [9] and also provides one with detailed information on the distribution function which could be useful for construction of a kinetic-fluid closure model [7, 24] for toroidal systems. For example, the profile of f_{k_x,k_y} for the most unstable mode ($k_y = 0.35$) in the turbulence shown in figures 6 and 7 also has a significant difference from the linear eigenfunction, which suggests that the phase-relation between the temperature and the parallel heat flux may not be fixed to a constant value governed by the linear eigenfunction, but can vary in time as is supposed in the nondissipative closure model [7, 24].

6. Summary

We have studied the detailed velocity–space structures of ion distribution functions and related entropy balance in the collisionless damping of the zonal flow and GAM as well as in the toroidal ITG turbulence with the anomalous ion

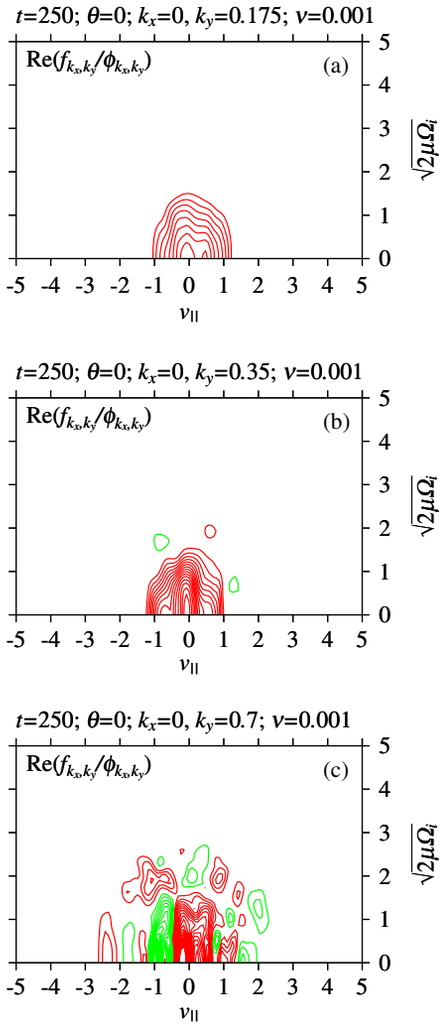

Figure 6. Velocity–space profiles of real part of the perturbed distribution function observed in the toroidal ITG turbulence simulation at $t = 250L_n/v_{ti}$ for (*a*) $k_y = 0.175$, (*b*) 0.35 and (*c*) $0.7\rho_i^{-1}$ where $\theta = z = 0$ and $k_x = 0$. The horizontal and vertical axes are defined by $v_\parallel$ and $\sqrt{2\mu\Omega_i}$, respectively. The contour interval in (*c*) is 0.04 but 0.02 in (*a*) and (*b*).

thermal transport, by means of the newly developed toroidal GKV simulation code for the flux tube geometry. The kinetic simulations with high velocity–space resolution enable us to quantitatively discuss the entropy balance which has rarely been evaluated in conventional studies. Our detailed numerical simulation on the dynamics of the axisymmetric modes reveal the whole picture of the collisionless damping of the zonal flow and GAM in association with the phase–space structures of the perturbed ion distribution function, δf. Specifically, the neoclassical polarization of trapped ions as well as the ballistic mode structures associated with collisionless particle motions are successfully reproduced. The velocity–space profile of the distribution function obtained by the simulations is also consistent with the analytical solution in equation (9). During the collisionless damping of GAM, the finer-scale structures of the distribution function in the velocity space continue to develop while preserving an invariant defined by a sum of the entropy variable and the potential energy. Thus, the collisionless dynamics of the zonal flow and GAM are

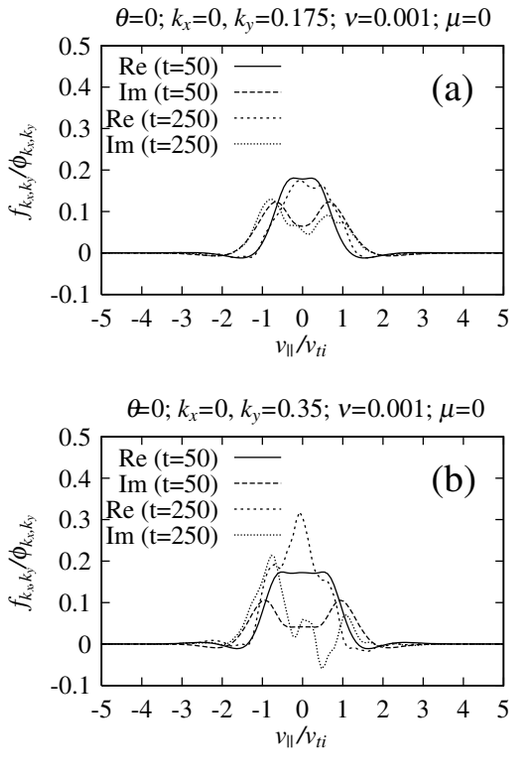

Figure 7. The cross-sectional plots of real and imaginary parts of the perturbed distribution function at $\mu = 0$ for (a) the longest wavelength ($k_y = 0.175\rho_{\rm i}^{-1}$) and ($b$) the most unstable ($k_y = 0.35\rho_{\rm i}^{-1}$) modes observed at $t = 50$ (linear growth phase) and $250L_n/v_{\rm ti}$ (nonlinear saturation phase).

comprehended in terms of a transfer process of the entropy variable from macro to micro velocity-scales.

It is considered that weak but finite collisionality leads to a slow decay of the residual zonal flow [25]. In addition, the entropy variable in the micro velocity-scale and the fine-scale structures of the distribution function are dissipated by collisions. Thus, a long time simulation also becomes possible at a smaller computational cost than that in the collisionless case. This is because collisionless kinetic simulations need a lot of computer resources in order to reproduce the fine structures of the distribution function and are reliable only in a finite time period before the smallest scale-length of δf in the phase–space reaches the grid scale [8]. Recently, the collisionless zonal flow dynamics in helical systems was also studied based on the gyrokinetic theory and simulation [26], where the velocity-space structures of the distribution function are quantitatively investigated. The detailed results will be reported elsewhere [27].

The simulation results of the anomalous transport in the toroidal ITG turbulence, with attention to the velocity–space structures of the distribution function and the entropy balance, are also presented. The statistically steady toroidal ITG turbulence is observed in terms of the saturated states of the entropy variable, the potential energy, the ion heat transport flux and the collisional dissipation. Detailed calculation of the entropy balance for the toroidal flux tube geometry confirms the steady state of the turbulence where the transport balances with the collisional dissipation in the same way as found in the slab ITG system [9]. Fine velocity–space structures of the perturbed ion distribution function clearly appear in fluctuations with large wave numbers, while the heat transport flux is mainly produced by vortices with long wavelengths. Accordingly, the entropy variable produced by the unstable modes with a macro velocity-scale is transferred in the wave number and velocity–spaces, and is finally dissipated in the micro scale by collisions. Thus, the statistically steady toroidal ITG turbulence can be sustained, as we have seen in the slab case.

Introduction of the finite collisionality also makes the long-time simulation of the turbulent transport possible by smoothing out the fine-scale structures of the distribution function. According to our previous studies on the slab ITG turbulence, the collision frequency used in the present study ($\nu_{\rm ii} = 10^{-3}v_{\rm ti}/L_n$) is in a regime where the transport flux has a logarithmic dependence on $\nu_{\rm ii}$. Even if one employs numerically-enhanced diffusivity instead of the collision term with coarser phase–space resolution so as to carry out a *collisionless* turbulence simulation for the same parameters as used here, the transport coefficient may deviate from that in the true collisionless limit. Therefore, in order to quantitatively study the collisionality dependence of the velocity–space structures of the distribution function, one needs to perform numerical simulations with higher phase–space resolution for a lower collision frequency, as well as those with different parameters ($\eta_{\rm i}$, $R_0/L_{\rm T}$, q_0, $\hat{s}$ and so on), which remains for future works.

In the present work, we have assumed the adiabatic electron response which constitutes the minimal gyrokinetic simulation model for the toroidal ITG turbulence. In order to study the particle and the electron heat transport, however, one should take into account the nonadiabatic response. The effects of kinetic electrons on the zonal flow and GAM [28], on the trapped electron mode turbulence [29] and on the finite β-scaling of transport [30] have been investigated as the next step of the adiabatic electron model for the electrostatic ITG turbulence. Our GKV simulation code will also be extended in future so as to include the nonadiabatic electron response as well as other multi-physics effects.

Acknowledgments

This work is supported in part by grants-in-aid of the Ministry of Education, Culture, Sports, Science and Technology (No. 14780387, 16560727 and 17360445) and in part by the National Institute for Fusion Science Collaborative Research Program (NIFS04KDAD003).

References

[1] Horton W. 1999 *Rev. Mod. Phys.* **71** 735
[2] Terry P.W. 2000 *Rev. Mod. Phys.* **72** 109
[3] Diamond P.H., Itoh S.-I., Itoh K. and Hahm T.S. 2005 *Plasma Phys. Control. Fusion* **47** R35
[4] van Kampen N.G. and Felderhof B.U. 1967 *Theoretical Methods in Plasma Physics* (Amsterdam: North-Holland)
[5] Krommes J.A. and Hu G. 1994 *Phys. Plasmas* **1** 3211
[6] Sugama H., Okamoto M., Horton W. and Wakatani M. 1996 *Phys. Plasmas* **3** 2379
[7] Sugama H., Watanabe T.-H. and Horton W. 2001 *Phys. Plasmas* **8** 2617
[8] Watanabe T.-H. and Sugama H. 2002 *Phys. Plasmas* **9** 3659

[9] Watanabe T.-H. and Sugama H. 2004 *Phys. Plasmas* **11** 1476
[10] Watanabe T.-H. and Sugama H. 2004 *J. Plasma Fusion Res. Ser.* **6** 23
[11] Rosenbluth R.M. and Hinton F.L. 1998 *Phys. Rev. Lett.* **80** 724
[12] Winsor N., Johnson J.L. and Dawson J.J. 1968 *Phys. Plasmas* **11** 2448
[13] Frieman E.A. and Chen L. 1982 *Phys. Fluids* **25** 502
[14] Beer M.A., Cowley S.C. and Hammett G.W. 1995 *Phys. Plasmas* **2** 2687
[15] Sugama H. and Horton W. 1997 *Phys. Plasmas* **4** 405
[16] Sugama H. 1999 *Phys. Plasmas* **6** 3527
[17] Dimits A.M. *et al* 2000 *Phys. Plasmas* **7** 969
[18] Lin Z. *et al* 2000 *Phys. Plasmas* **7** 1857
[19] Candy J. and Waltz R.E. 2003 *J. Comput. Phys.* **186** 545
[20] Idomura Y., Tokuda S. and Kishimoto Y. 2003 *Nucl. Fusion* **43** 234
[21] Hairer E., Nørsett S.P. and Wanner G. 1993 *Solving Ordinary Differential Equations I* (Berlin: Springer-Verlag)
[22] Clemmow P.C. and Dougherty J.P. 1969 *Electrodynamics of Particles and Plasmas* (Redwood City: Addison-Wesley)
[23] Xu X.Q. and Rosenbluth M.N. 1991 *Phys. Fluids* B **3** 627
[24] Sugama H., Watanabe T.-H. and Horton W. 2003 *Phys. Plasmas* **10** 726
[25] Hinton F.L. and Rosenbluth R.M. 1999 *Plasma Phys. Control. Fusion* **41** A653
[26] Sugama H. and Watanabe T.-H. 2005 *Phys. Rev. Lett.* **94** 115001
[27] Sugama H. and Watanabe T.-H. 2005 Collisionless dumping of zonal flows in helical systems *Phys. Plasmas* at press
[28] Parker S.E., Chen Y., Wan W., Cohen B.I. and Nevins W.M. 2004 *Phys. Plasmas* **11** 2594
[29] Ernst D.R. *et al* 2004 *Phys. Plasmas* **11** 2637
[30] Candy J. 2005 *Phys. Plasmas* **12** 072307